High-Frequency Paleovariability in Climate and CO2 Levels From Vostok Ice Core Records

Pascal Yiou, C. Genthon, M. Ghil, J. Jouzel, H. Le Treut, J. Barnola, C. Lorius, Y. Korotkevitch

High-Frequency Paleovariability in Climate and CO$_2$ Levels From Vostok Ice Core Records

P. Yiou,[1,2] C. Genthon,[1] M. Ghil,[2] J. Jouzel,[1,3] H. Le Treut,[4] J. M. Barnola, [3] C. Lorius,[3] and Y. N. Korotkevitch[5]

The high resolution of the Vostok records provides a unique look at the causes of paleoclimatic variability during the last complete glacial cycle. The records present strong evidence for the interaction between orbital forcing and internal, physico-chemical mechanisms of variability. This interaction appears to account for the great wealth of spectral features found in the records.

1. Introduction

The Quaternary glaciation cycles of the last 2 million years represent a particularly interesting and important problem for the study of climatic change: interesting because of the wealth of data, isotopic, microfaunal and geologic, accumulated, and important because of the relatively large amplitude and suddenness of changes in global temperature, ice volume and other climatic parameters involved [*Imbrie and Imbrie*, 1986]. Understanding these large and rapid changes in the recent geologic past should help us to understand current changes and predict future ones. A key question for understanding and predicting climatic change is the relative importance of external and internal factors in the change.

The insolation changes due to variations in the Earth's orbit around the Sun are a paradigmatic example of an external cause of climatic change [*Milankovitch*, 1941; *Berger*, 1978]. The role of orbital factors was put on a solid foundation by the pioneering work of *Hays et al.* [1976] and by the extensive follow-up research of the Climate: Long-Range Investigation, Mapping, and Prediction (CLIMAP) and SPECMAP projects [*Imbrie et al.*, 1984]. Serious questions remain, however, about the possible role of complementary, internal factors, and we list a few of the facts suggesting that this role must have been important. Orbitally induced insolation cycles have been documented for pre-Quaternary times, when climate was much warmer on the average and its variation much smaller [*Anderson*, 1982; *Olsen*, 1986]. All three orbital parameters which determine insolation, eccentricity, obliquity and precession, had values at the last glacial maximum which are almost identical to the present [*Held*, 1982; *Saltzman*, 1985]. Glaciations have rapid terminations, while insolation varies smoothly, and they occur almost simultaneously in both hemispheres, while insolation in the two differs greatly [*Broecker*, 1984; *Nelson et al.*, 1985]. Finally, rapid events of almost full glacial-to-interglacial extent and very short duration, such as the Alleröd-Younger Dryas, are now well documented at least for the Holocene [*Duplessy et al.*, 1981; *Broecker et al.*, 1985; *Bard et al.*, 1987] and are of global extent [*Jouzel et al.*, 1987; *Kallel et al.*, 1988].

To advance our knowledge of climatic variability due to internal factors, and of its interaction with climatic response to orbital forcing, it is necessary to apply refined tools of time series analysis to continuous, high-resolution records of paleovariations in climate and atmospheric CO$_2$. The Vostok ice core records span over 164,000 years and cover the last glacial and the preceding interglacial. The spectral analysis of some of these records permits the study of high frequencies, i.e., of periods between 2 kyr and 20 kyr (1 kyr = 1000 years). We chose a novel, nonparametric method with excellent spectral properties (due to *Thomson* [1982]) to investigate the presence of high frequencies, and evolutive analysis to study the change in time of their amplitudes. Fairly stable cycles appear at 11.1, 6.0, 4.4, 3.5, 2.7, and 2.4 kyr. These cycles are distinct from the orbital periodicities at 41, 23, and 19 kyr, also present in the records, and appear to be related to harmonics and combination tones of the latter. This confirms the role of nonlinear physico-chemical interactions in explaining paleoclimatic variability. Nonlinear mechanisms of particular importance are ice-albedo feedback, precipitation-temperature feedback, ice-sheet/bedrock interactions and changes in atmospheric chemical composition.

2. The Vostok Ice Core Records

The purpose of this paper is to examine paleoclimatic high frequencies between 1/20 kyr and 1/2 kyr. Long ice cores permit such an investigation owing to their high-resolution sampling, which puts the Nyquist frequency of the time series outside this frequency band.

The Vostok ice core was drilled in East Antarctica, at the Soviet station Vostok (78°28'S, 106°48'E) from an altitude of 3488 m, and has a total length of 2083 m [*Lorius et al.*, 1985]. Ice samples were analyzed with respect to isotopic content in deuterium [*Jouzel et al.*, 1987] and in oxygen 18 [*Lorius et al.*, 1985], as well as to carbon dioxide trapped in air bubbles [*Barnola et al.*, 1987]. The isotopic abundance ratios of D and ^{18}O were expressed as usual in per mil deviation, δD and δ^{18}O, from standard mean ocean water.

δD and δ^{18}O at Vostok both reflect surface temperature and are currently translated into it by using a linear relationship [*Lorius and Merlivat*, 1977; *Jouzel and Merlivat*, 1984],

VOSTOK : CO_2 and Temperature

Fig. 1. Surface temperature (difference in degrees Celsius from the modern value $T_0 = -55.5°C$, along the vertical axis on the right) as deduced from deuterium content and smoothed by a cubic spline, and CO_2 time series at Vostok (adapted from [Barnola et al., 1987] and given in parts per million by volume along the vertical axis on the left).

with a slight correction for the change in isotopic content of oceanic water. Moreover, the three profiles of δD, $\delta^{18}O$ and CO_2 behave all three in a similar way with respect to depth in core, showing a short interglacial stage, the Holocene, at the top, a long glacial stage below, and the last interglacial stage near the bottom of the core (see Figure 1). Still, the record sampling in D is finer than in ^{18}O or CO_2 and δD is a slightly better indicator of changes in temperature [Jouzel et al., 1987]. Hence we focus on the study of the temperature profile derived from δD measurements, keeping in mind that a finer sampling in CO_2, if it were possible, might give similar results.

The chronology of the core was established by using a snow accumulation model and a two-dimensional ice flow model [Lorius et al., 1985]. We accept provisionally this chronology as a case study for the effect of perturbations in the dating on the evolutive spectra, but we keep in mind that this chronology might need refinements, according to recent Vostok dust data [Petit et al., 1990]. With a given chronology, the δD profile yields a time series spanning approximately the last 160 kyr. The time sampling Δt is very fine, varying from 50 years near the top of the core to 800 years, due to a single hiatus, with an average Δt of 100 years. The surface temperature T_δ is calculated directly and very reliably from the δD time series, providing an excellent, highly resolved paleoclimatic time series $T_\delta(t)$.

Jouzel et al. [1987] carried out a spectral analysis of the surface temperature record at Vostok using a maximum entropy method (MEM) with a very large number of lags. Their analysis confirmed the presence of orbital periods near 41 and 23 kyr in the record with good accuracy, but they postponed the study of high frequencies, since their importance warranted a separate investigation and because of the limitations of the MEM method. Pestiaux et al. [1988] used MEM with varying lags to yield high frequencies in marine cores with large sedimentation rates. Confidence intervals for MEM algorithms, however, are difficult to obtain [Kay and Marple, 1981]. Moreover, MEM spectra are sometimes affected quite severely by the choice of the number of lags for

short time series. Hence we use a nonparametric robust spectral method, presented in the next section.

3. Spectral Analysis: A New Approach

The time series at our disposal, $T_\delta(t)$, has an average sampling interval of $\Delta t \approx 0.1$ kyr and a total length of $\overline{T} \approx 164$ kyr. It is short with respect to the reliable detection of the obliquity peak at 41 kyr in the global spectrum and is also short for the purposes of evolutive spectral analysis. Indeed, we want to compare the stability of high frequencies, i.e., of periods from 2 to 20 kyr approximately, with the stability of orbital peaks, by using a sliding window, 40 kyr long.

The Multitaper Method (MTM)

This method uses an optimal set of tapers [Thomson, 1982] instead of the single, empirical ones available until recently (see also Slepian [1978], Park et al. [1987], and Appendix A). Besides its high resolution, the MTM method provides a statistical F test for the validity of the location of each peak in the spectrum and for its amplitude. Hence this method can detect with a high degree of confidence low-amplitude oscillations which would have been missed entirely or detected with only questionable reliability by other methods [Thomson, 1982].

We tested the MTM method on simulated time series and compared the results to MEM and to the Blackman-Tukey (B-T) autocorrelation method. The tests showed that MTM offers indeed the best spectral resolution and does not yield spurious peaks. For the B-T method, statistical significance of a peak is highly correlated with its amplitude. This is not necessarily so for MTM [Thomson, 1982], and in the sequel we concentrate on the F test value for each spectral peak, which measures our statistical confidence in the peak. The value of the F test varies smoothly in time, while the amplitude of a peak does not [Pestiaux, 1984].

Evolutive Spectral Analysis (ESA)

This approach was used in paleoclimatology by Pestiaux [1984] in conjunction with a MEM method to verify the stability of orbital peaks in marine cores. He showed that these peaks are stable even when using absolute dating techniques, independent of the tuning to orbital time series proposed by Imbrie et al. [1984]. Pestiaux's work, in addition to the arguments of Lorius et al. [1985], justifies our use of an absolute chronology as the basis for our spectral studies.

In ESA, one studies the evolution of the local spectrum in time when taking a window of given length and moving it along the time series. This analysis provides valuable information since internal mechanisms can be triggered or amplified at one time and vanish some time later, inducing the appearance of one or more new peaks for some interval of time. Such internal variability is typical of nonlinear systems [Lorenz, 1968; Ghil and Childress, 1987]. Global spectral analysis would not capture such a process.

The analysis we perform creates a map of the evolution of the F test value with time, along the Vostok ice core. We take a window of length $2T$ beginning at time $t_0 - T$, such that $t_0 - T = 0$ ka (ka = kyr before present), i.e., $t_0 = T$, and ending at time $t_0 + T$. MTM analysis is performed on the first time series of length $2T$. The window is then shifted by a lag τ and MTM is carried out on this second time series,

from $t_0 + \tau - T$ till $t_0 + \tau + T$. The operation is repeated until we reach the end of the time series, the last window extending from $\hat{T} - 2T$ until $\hat{T}$. Thus we obtain a three-dimensional (3D) representation of F test values: one axis represents the center t of the time windows, a second axis stands for frequency, and the third axis gives the F test value. This 3D representation is projected onto a two-dimensional (2D) contour map of values.

For a simulated signal given by a finite sum of sinusoids with arbitrary frequencies, the contour map thus obtained would show sharp ridges of nearly constant height parallel to the time axis and centered on the given frequencies. This would also be the case if the climatic system were linear, as postulated by *Imbrie et al.* [1984], and all or most of its variability were forced by the orbital changes. A nonlinear dynamical system, however, can undergo bifurcations, i.e., changes in spectrum as a parameter changes [*Guckenheimer and Holmes*, 1983; *Ghil and Childress*, 1987]. On longer time scales, such changes of spectral behavior between early and late Pleistocene have been observed [*Pisias and Moore*, 1981] and argued to represent internal bifurcations by *Ghil* [1984] and by *Saltzman and Sutera* [1987]. No such observations have been made as yet for the last full climatic cycle, analyzed here.

4. HIGH-RESOLUTION SPECTRAL RESULTS

Global Analysis Results

Thomson's [1982] MTM method was applied to the temperature time series $T_\delta(t)$ calculated from the δD record [*Jouzel et al.*, 1987] at Vostok. More precisely, we study $\theta(t) \equiv T_\delta(t) - T_0$, which is the difference between the paleotemperature T_δ and the present surface temperature T_0 at Vostok, $T_0 = -55.5°C$.

The MTM method, like other spectral methods, requires a regularly sampled time series. Hence we interpolate the data by cubic splines. This provides an optimized version, in the sense of least squares or of linear regression, of the given time series over a regular grid, and appears to be, in our experience, an improvement over the customary linear interpolation.

First, we calculate the MTM spectrum of the entire time series over a broad frequency band, from 0 to 0.1 cycles/kyr (Figure 2a). The spectrum exhibits peaks superimposed on a continuous background, like those of other paleoclimatic time series, analyzed by other spectral methods [*Ghil and Childress*, 1987]. In general, both peaks and background decrease in variance with increasing frequency. This pervasive property of "warm" noise [*Le Treut et al.*, 1988], encountered here as for most paleoclimatological and geophysical spectra, justifies the use of high-pass filters, e.g., prewhitening [*Jenkins and Watts*, 1968], for the ESA study of high frequencies over short time windows.

Peaks near the orbital periodicities, at 41.7, 24.1, and 18.3 kyr, are clearly noticeable in amplitude (thick curve) and have a statistical significance over 90% (thin curve). This confirms the results of *Jouzel et al.* [1987], who used MEM, and emphasizes that the basic chronology of *Lorius et al.* [1985], while independent of any orbital tuning, is not at variance with orbital insolation effects on global climate. In fact, the MEM analysis of *Jouzel et al.* [1987] only detected two orbital peaks, corresponding to the obliquity period 41 kyr and to one precessional period, 23 kyr. Our analysis

yields also the second precessional peak, near 19 kyr, for the same data, illustrating the superiority of the MTM method.

For convenience, the three uncontroversial orbital frequencies associated with the precessional parameter $\varepsilon \sin \omega$ and the obliquity α will be denoted, in the increasing order of the associated periodicities, by $f_1 = 1/19$, $f_2 = 1/23$ and $f_3 = 1/41$, in cycles per kiloyear [*Ghil and Childress*, 1987]. In addition to these three, there is a highly significant peak at 133 kyr, which could easily be seen on the time series itself. This peak corresponds to a single cycle within the record; it is given essentially by the estimated time interval between terminations I and II in the record and is therefore highly dependent on the chronology of choice. But for no chronology in use can it be attributed exclusively to eccentricity forcing (see also *Winograd et al.* [1988] for even earlier dates of termination II).

Sharp peaks at shorter periods, 16, 14.1, and 11.1 kyr are also in evidence. While their amplitude is smaller, their statistical significance is quite high and comparable to that of the orbital peaks approximating f_1, f_2, and f_3 in the record. In fact, the F test value of the peak at 11.1 kyr is equal to that of the low-frequency peak at 133 kyr, and much larger than that of the purely orbital peaks f_1, f_2, and f_3. The peak at 11.1 kyr and the one at 14.1 kyr approximate very well harmonics and sum tones of the orbital frequencies, $2f_2$ and $f_2 + f_3$, respectively.

The presence of such combination tones, as a result of interactive nonlinearities within the climatic system, was predicted by *Le Treut and Ghil* [1983], based on the simple nonlinear climate model of *Ghil and Le Treut* [1981] (GLT hereinafter); these combination tones were further analyzed by *Ghil* [1985], *Ghil and Childress* [1987, section 12.5], and *Le Treut et al.* [1988]. For comparison purposes the MTM spectrum of the GLT model is shown in Figure 2b, for the same frequency band as that of the Vostok record in Figure 2a. Model parameters are chosen to coincide with those of *Le Treut et al.* [1988], and the length of the simulated record is also 164 kyr.

The spectral peaks in the model and the peaks in the record are in good correspondence with each other. The orbital peaks f_1, f_2, and f_3 appear clearly in both. The suborbital, low-frequency peak near 100 kyr is due in the GLT model [*Ghil and Le Treut*, 1981; *Le Treut and Ghil*, 1983; *Ghil*, 1985] to a difference tone between the two precessional peaks, $f_1 - f_2$. It approximates rather well the mean periodicity of the seven terminations between the Brunhes-Matuyama boundary, at 730 ka ± 20 kyr, and the present [*Broecker*, 1984; *Imbrie and Imbrie*, 1986; *Ghil and Childress*, 1987], namely, 104.3 kyr. It is also quite close to the peak at 107.5 kyr obtained by *Jouzel et al.* [1987], using MEM (their Figure 3). The irregularity of the time intervals between terminations, in the model as well as in long marine cores, is due to the presence of "warm" noise, common to model and data [*Le Treut and Ghil*, 1983; *Ghil*, 1985; *Ghil and Childress*, 1987; *Le Treut et al.*, 1988]. Hence the Vostok record, spanning as it does only one full glacial-interglacial cycle, is not suitable for the spectral study of suborbital frequencies like $f_1 - f_2$. Such a study requires a few complete cycles at least to average over and is better done on marine cores, subject to reliable dating.

In the superorbital, or high-frequency range between f_1 and 0.1 cycles/kyr, four peaks appear in the model at 15, 13.2, 11.6, and 10.4 kyr, and three in the data, at 16, 14.1,
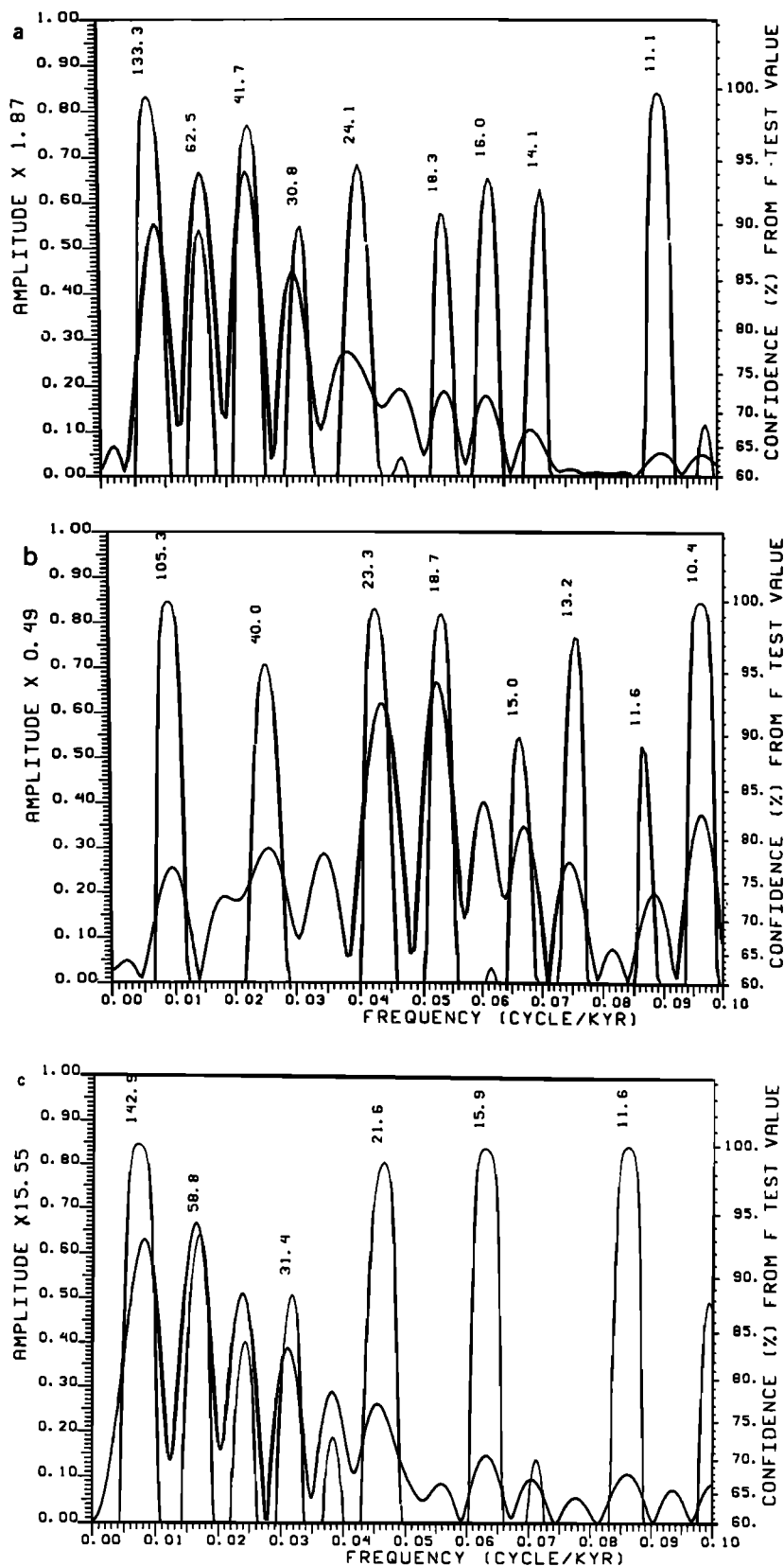
Fig. 2.   (a) MTM analysis of the entire temperature time series at Vostok. The thick curve represents the amplitude (left axis) and the thin curve represents the confidence value in percent (right axis). (b) MTM analysis of the temperature from the Ghil-Le Treut (GLT) model [*Ghil and Le Treut*, 1981; *Le Treut and Ghil*, 1983]. The time series analyzed is 164 kyr long and sampling is at 0.5 kyr. (c) MTM analysis of the CO_2 time series at Vostok. The frequency band is 0 to 0.1 cycles/kyr in all three panels.

and 11.1 kyr. This is not a perfect fit, but the situation is quite comparable to that encountered many times for the orbital peaks themselves. *Hays et al.* [1976] found in most of their spectra only two, rather than three orbital peaks (their Figures 5 and 6), with substantial fluctuations (up to 5% relative error in period) in their position. *Jouzel et al.* [1987], using MEM, also found only two orbital peaks (their Figure 3) in the time series analyzed here. Two orbital peaks only appear in the spectrum of the CO_2 time series at Vostok, either by MEM [*Barnola et al.*, 1987] or by MTM (Figure 2c here). Hence the mild discrepancy between the superorbital peaks in Figures 2a and 2b can be attributed, like that for the orbital ones, to imperfections in the records and in the chronology. The latter can be estimated not to exceed 5–10% [*Lorius et al.*, 1985; *Jouzel et al.*, 1987], which is entirely consistent with the observed differences between the two figures. The excellent qualitative and reasonably good quantitative agreement between model and data suggests, at least, that the oscillatory interactions between ice-albedo feedback, temperature-precipitation feedback and ice load/snow accumulation feedback on which the GLT model is based play an important role in the glaciation cycles of the Quaternary. This conclusion, very tentative so far, will be corrobotated by further evidence below.

In addition to the spectral features discussed already, the isotopic temperature data exhibit two peaks, at 62.5 and 30.8 kyr, which do not appear to be related to the orbital peaks themselves nor to their combination tones, and have a statistical significance just under 90%. The higher frequency of the two is almost the second harmonic of the lower one. They could be simply the second and fourth harmonic of the low frequency at 1/133 cycles/kyr. But 62.5 kyr is well within the range of free self-sustained oscillations of the *Birchfield and Grumbine* [1985] ice sheet/bedrock model, based on the nonlinear interaction between ice-mass balance, viscoplastic ice flow and viscoelastic adjustment of the bedrock under the ice load. These mechanisms are also present in the GLT model but play a less crucial role there.

To verify whether these two peaks are harmonics of the largest peak in the record or not, we also perform MTM analysis on the Vostok CO_2 time series [*Barnola et al.*, 1987] (Figure 2c). The two time series must represent the same physically interacting phenomena, and the same age model is used for both, except for a small additional correction to the age of the CO_2 in the air bubbles, which leaves an uncertainty of about 1 kyr in the CO_2 chronology with respect to δD. Hence the peaks in the two spectra should coincide in frequency, although not in amplitude [*Ghil*, 1985; *Le Treut et al.*, 1988]. The extent to which the frequencies differ between the CO_2 and the temperature records gives an indication of the effects of short record length on the accuracy of the estimates.

In the CO_2 spectrum, significant peaks appear near 143, 59, 22, 16, 12, and 10 kyr. The first three peaks can be related to those at 116, 55, and 21 kyr obtained by MEM by *Barnola et al.* [1987] but are probably more accurate. The difference in frequency between most of the CO_2 peaks here (Figure 2c) and the corresponding temperature peaks (Figure 2a) is no larger than that between either record and the GLT model simulation (Figure 2b), having the same length. The only peaks for which this statement does not hold are the peak near 100 kyr, for reasons discussed already, and the peaks which are not in one-to-one correspondence between the

three panels. With this caveat, the largest relative differences $\Delta f/f$ between the three pairs of panels are 0.07 (Figures 2a and 2c, five peaks), 0.12 (Figures 2a and 2b, five peaks) and 0.08 (Figures 2b and 2c, three peaks).

The peak at 58.8 kyr in the CO_2 record has higher significance than in the temperature and appears even more remote from a second harmonic of the "fundamental" at 143 kyr. A peak near 31 kyr is also present in the CO_2 record, with a significance of 88%. A peak at 31 kyr was found by *Pisias and Rea* [1988] in a marine record from the central equatorial Pacific, RC11-210, spanning the last 850 kyr. These authors attributed the peak to a sum tone of the dominant period in their record, namely, 100 kyr, and the obliquity peak at 41 kyr, also present in their low-latitude data. A peak at 64.5 kyr was also found by singular spectrum analysis in the $\delta^{18}O$ record of marine core V28-239 [*Shackleton and Opdyke*, 1976] by *Ghil* [1989] and *Vautard and Ghil* [1989], who tentatively attributed it to the oscillatory interaction between northern hemisphere ice sheets and the underlying bedrock, as modeled by *Birchfield and Grumbine* [1985]. The combined evidence from these two marine cores, RC11-210 and V28-239, and from our two Vostok records, temperature and CO_2, would seem to favor 31 kyr as the second harmonic of 62.5 kyr. Since the peak near 100 kyr is strongly shifted to the left in the Vostok records, and the peak near 41 kyr has very low significance in the CO_2 record, both the peak near 60 kyr and its harmonic near 30 kyr appear to be due to ice sheet/bedrock interactions [*Birchfield and Grumbine*, 1985]. These interactions may act in turn through both global albedo and sea level changes [*Peltier*, 1982] on equatorial sea surface temperature [*Pisias and Rea*, 1988] and on atmospheric CO_2 levels [*Barnola et al.*, 1987].

The presence of frequencies higher than the orbital ones in both the GLT model and the Vostok temperature record suggests pushing the investigation toward still higher frequencies. In particular, it is well known from previous studies of ice cores from Greenland [*Dansgaard et al.*, 1971] and from other parts of Antarctica [*Benoist et al.*, 1982] that a peak near 2.5 kyr is quite prominent in $\delta^{18}O$ records from the ice. Hence we consider in Figure 3 frequencies between 0.1 and 0.65 cycles/kyr. This part of the investigation is restricted to the temperature record, since CO_2 could only be sampled at an average interval of 2.6 kyr [*Barnola et al.*, 1987]. Sharp peaks at 7.35, 6.57, 5.43, 4.90, 4.35, 3.82, 3.65, 3.47, 3.36, 2.45, and 2.38 kyr appear in the Vostok temperature record (Figure 3a). All of these, except two, can be explained in terms of combination tones of f_1, f_2, and f_3 (see Table 1).

Pestiaux et al. [1988] found similar results in marine cores, with a combination of the MEM and B-T methods. We improve here on their results in three ways. First, the resolution of the δD profile at Vostok is better than that of $\delta^{18}O$ in the three Indian Ocean cores used by *Pestiaux et al.* [1988] which had Nyquist periods of 1.2 kyr at best. Second, the MTM method allows one to estimate the statistical significance of each peak detected, which MEM does not. Third, we give, following *Ghil* [1989], a quantitative evaluation of the precision with which each selected peak can be expressed as a combination tone of orbital frequencies. Let

$$r_i = \left| f_i^{(d)} - \sum_{j=1}^{3} n_j^{(i)} f_j \right|$$
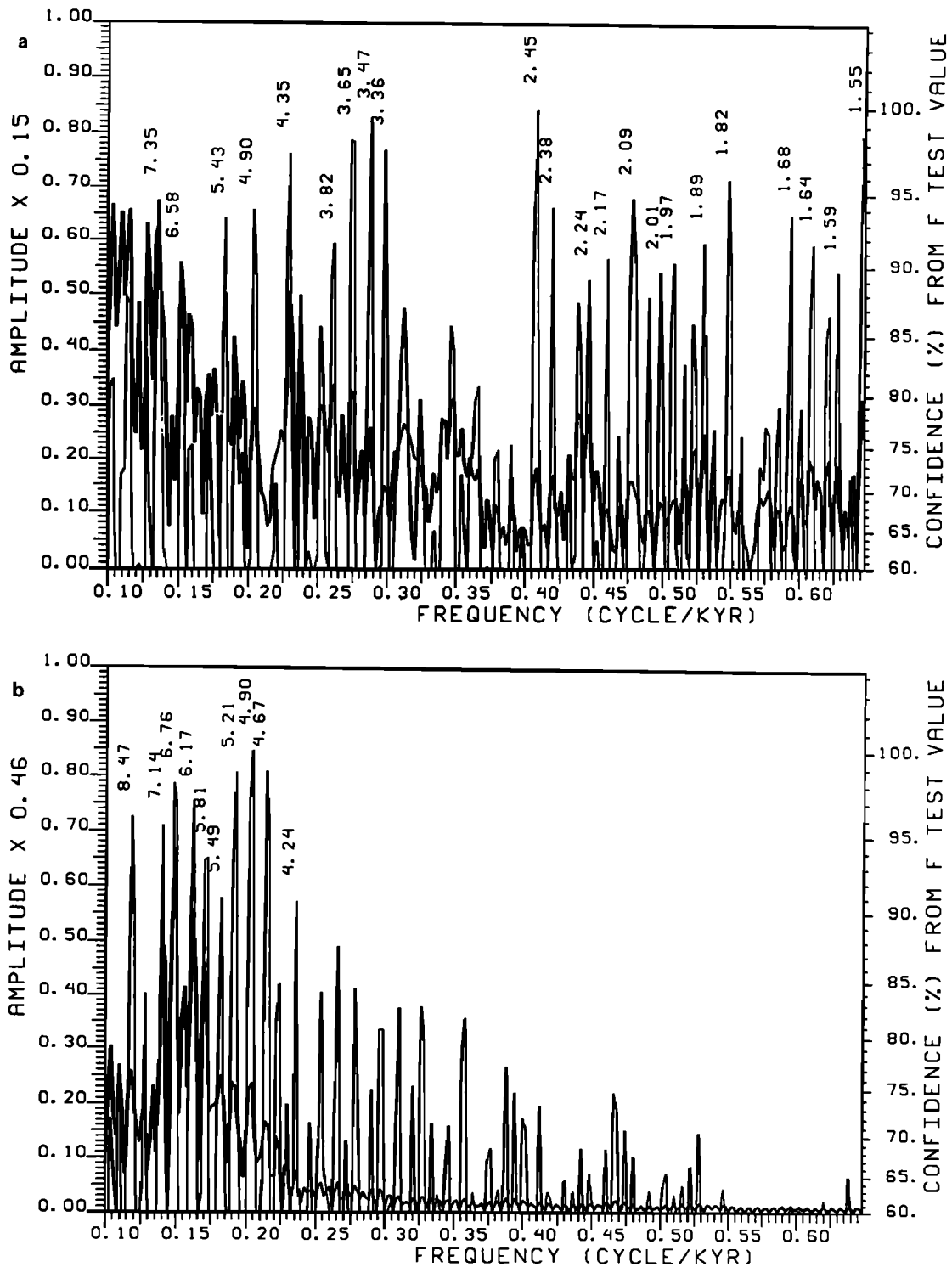
Fig. 3. (a) MTM analysis of the temperature time series at Vostok for higher frequencies. Thick and thin curves as in Figure 2. (b) MTM analysis of the temperature time series from the GLT model. The frequency band is 0.1–0.65 cycles/kyr in both panels.

be the residual of approximating the detected frequency $f_i^{(d)}$ by a combination tone with coefficients (n_1, n_2, n_3), and let

$$N_i = \sum_{j=1}^{3} |n_j^{(i)}|$$

be the order of the combination. The lower N_i, as well as r_i, the better approximation. In Table 1 are listed, for each peak with statistical significance above 90%, both r_i and N_i.

Clearly, as $f_i^{(d)}$ increases, so does N_i. But it is remarkable that this increase is monotone (except for the peaks at 16, 3.82, and 3.65 kyr) and that the order N_i does not exceed for

TABLE 1.   Statistically Significant Frequencies in the Vostok Temperature Record

Period, kyr	Frequency, cycles/kyr	Statistical Significance, %	Combination Tone	Relative Error*	Order of Combination
133.	0.0075	99			
41.6	0.024	97	f_3	1×10^{-2}	1
24.1	0.041	94	f_2	4×10^{-2}	1
18.3	0.054	90	f_1	3×10^{-2}	1
16.0	0.062	93	$2f_2 - f_3$	2×10^{-3}	3
14.1	0.071	93	$f_2 + f_3$	4×10^{-2}	2
11.1	0.090	99	$2f_2$	3×10^{-2}	2
7.35	0.136	94	$2f_2 + 2f_3$	2×10^{-3}	4
6.57	0.152	90			
5.43	0.184	93	$f_1 + 3f_2$	5×10^{-3}	4
4.90	0.204	94	$3f_2 + 3f_3$	2×10^{-3}	6
4.35	0.230	97	$3f_1 + 3f_3$	4×10^{-3}	6
3.82	0.262	91	$5f_1$	3×10^{-3}	5
3.65	0.274	98	$3f_1 + f_2 + 3f_3$	2×10^{-3}	7
3.47	0.288	99	$3f_1 + 3f_2$	3×10^{-4}	6
3.36	0.298	97	$4f_1 + 2f_2$	2×10^{-3}	6
2.45	0.408	99			
2.38	0.420	94	$8f_1$	2×10^{-3}	8

The frequencies listed have a confidence of 90% or better.

*The relative error $r_i/f_i^{(d)} = (|f_i^{(d)} - \Sigma_{j=1}^3 n_j^{(i)} f_j|)/f_i^{(d)}$ is the absolute error, or residual, r_i, standardized by the observed frequency $f_i^{(d)}$.

any high-frequency peak $f_i^{(d)}$ the order of the orbital peaks' pure harmonics bracketing $f_i^{(d)}$. This monotonicity in order is due to the coefficients being positive (except for the peak at 16 kyr). Furthermore, the relative errors for the combination tones do not exceed those for the orbital peaks themselves. Our residuals for the latter are, in fact, quite comparable to the residuals obtained by other authors in marine cores from all oceans, as long as no orbital tuning was applied to the chronologies. Hence we should trust these combination tones no less than we trust the presence of orbital peaks in the records.

Still it might appear that by increasing the order of the combination tone any observed frequency could be approximated to within a prescribed accuracy by such a tone. This is known to be true if negative coefficients are permitted, but less clear when restricting the integer coefficients of the frequencies to be positive. We check therefore the probability that all the nonorbital frequencies detected by MTM in the Vostok temperature record could be ascribed by chance to combination tones with positive coefficients of the order given in Table 1. In Table 2 are listed the periods associated with each order, the cumulative absolute errors made at each order in approximating the corresponding frequencies by combination tones, and the probability that these frequencies be approximated with the given accuracy by combination tones due to pure chance. Notice that the cumulative error is of comparable size for all orders, including the orbital frequencies themselves (order 1), and that the probability of all the frequencies observed not being combination tones of the given orders is vanishingly small.

The MTM spectrum for the GLT model is given, for comparison purposes, in Figure 3b, over the same frequency band as in Figure 3a. Model parameters are the same as in Figure 2b. All the lines here are exact combination tones of the orbital frequencies, to within the effect of using a finite time series, and they match rather well the lines present in the temperature record for periodicities between 10 and 4 kyr. Le Treut et al. [1988] have shown that the power

spectrum of the GLT model decays quite rapidly for shorter periods, since the model's internal variability is concentrated near 10 kyr. It is likely therefore that the peaks observed in the data between 3 and 1.5 kyr are due to the agency of other climatic feedbacks mechanisms, with shorter characteristic times. In any case they cannot be attributed directly to orbital forcing, nor to other causes external to the climatic system.

The GLT model is governed by three nonlinear, deterministic, coupled ordinary differential equations governing global temperature, global ice volume and bedrock deflection under the load of an axisymmetric continental ice sheet. It might appear surprising that such a simple model, with only three degrees of freedom, can predict the presence of so many spectral regularities in the band between 40 and 4 kyr, confirmed now in ice core, as well as in marine core records. But the careful quantitative evaluation of the information content of $\delta^{18}O$ records in four marine cores suggests that the total number of statistically significant degrees of freedom present in these records is of only 5–10 [Vautard and Ghil, 1989; Ghil, 1989]. A similar evaluation for ice cores will be presented in a separate publication; preliminary results agree roughly with the estimate from the marine cores.

ESA Results

We now subject the peaks detected by MTM analysis of the entire ice record to a further test, by examining their dynamic stability. Visual inspection of the T_δ profile (Figure 1) shows clearly that a larger amount of high-frequency variance is present during the Holocene (stage A of Lorius et al. [1985]) and during part of the interstadial stage E (compare similar behavior of GLT model in Figure 6 of Le Treut et al. [1988] and discussion thereof; analogous behavior predicted by the model for stage G, the preceding interglacial, is probably suppressed in the core by the much greater compression of the ice near the bottom). It is natural therefore to apply the ESA approach to the Vostok temper-

TABLE 2. Probability of Obtaining Combination Tones by Pure Chance

Order N	Possible Combination Tones*	Period, kyr	Absolute Error,† $\times 10^{-4}$	Cumulative Error,† $\times 10^{-4}$	Theoretical Probability,‡ P_N or P
1	3	41.6	4		
		24.1	20		
		18.3	(20)	44	0.010
2	6	14.1	30		
		11.1	(30)	61	0.102
4	15	7.35	3		
		5.43	(9)	14	0.014
5	21	3.82	(12)	12	0.178
6	28	4.90	4		
		4.35	(11)		
		3.47	3		
		3.36	5	26	0.033
7	36	3.65	(5)	5	0.008
8	45	2.38	(10)	10	0.199
Total ($N \geq 2$)	151			128	1×10^{-8}

*There are $\nu_N = (N + 1)(N + 2)/2$ possible combination tones of order N, given three basic frequencies f_j, $1 \leq j \leq 3$, and positive coefficients $n_j^{(i)}$ only. We consider here only those $f_i^{(d)}$ for which $n_j^{(i)} \geq 0$. The ν_N combination tones $\{\Sigma_{j=1}^{3} n_j f_j\}$ of order $\Sigma_{j=1}^{3} n_j = N$ all have to lie between $N f_3$ and $N f_1$, since $f_3 < f_2 < f_1$.

†The absolute error equals the residual r_i defined in the text for each observed frequency $f_i^{(d)}$. The cumulative error c_N is the sum of the absolute errors for a given order N, $c_N = \Sigma_i r_i$, where the sum is over all i such that $\Sigma n_j^{(i)} = N$. The largest absolute error R_N for a given order N is given in parentheses.

‡Each approximation of a given frequency $f_i^{(d)}$ by a combination tone is considered here to be an independent random event. Let us say that frequency $f_i^{(d)}$ is found to lie between $N f_3$ and $N f_1$, where $N_i \equiv \Sigma_{j=1}^{3} n_j^{(i)} = N$. The probability p_i that this frequency be attributed by chance to a combination tone of order N with absolute error r_i is then no larger than $q_N = \nu_N R_N / N(f_1 - f_3)$ (where R_N is in parentheses). The m_N observed frequencies $f_i^{(d)}$ associated in the table with order N, $m_N \leq \nu_N$, differ by more than R_N from each other. Hence the probability that all m_N frequencies be approximated by chance using combination tones of that order is no larger than $P_N = q_N^{m_N}$; this is the number given in the last column for each order. If the eight frequency intervals $(N f_3, N f_1)$ for $N = 1, 2, \cdots, 8$ were disjoint from each other, the total probability for all the combination tones of order $N \geq 2$ in the table being attributed by chance to the observed frequencies would be no larger than $P = P_2 P_3 \cdots P_8 = 1 \times 10^{-8}$. Since there are overlaps (which leads in particular to the only two cases of nonmonotonicity in the table, with periods 3.82 kyr and 3.65 kyr being associated with orders 5 and 7, rather than 6, respectively), a slightly more refined calculation is necessary. The resulting upper bound on the joint probability of all observed frequencies being attributed by chance to combination tones with positive coefficients is $P' = 7 \times 10^{-8} > P$. The probability therefore that at least one of the nonorbital frequencies be a combination tone is no less than $1 - P' = 0.99999993$, i.e., this is, for all practical intents and purposes, certain to be the case.

ature time series and to explore the stability of the peaks in time, as well as the correlation between their statistical significance at different times and the visual evidence.

As shown before, the orbital peaks have larger amplitudes than the high-frequency peaks of interest here. Thus when taking a short potion of the Vostok signal, the high frequencies will be drowned by the tendency associated with the lower ones. We prewhitened therefore the signal with a first-order filter so as to remove the low-frequency components.

We chose, after trial and error, to take windows of 40 kyr, which offer a good compromise between stability and resolution. Indeed, if the window is too small, the frequency resolution will be poor; on the other hand, too large a window will not provide a sufficient set of local spectra for intercomparison. Thus 40-kyr windows were found to be preferable to 20-, 30-, and 50-kyr windows. The time shift τ is taken equal to 10 kyr, which gives a sufficient number of spectra to provide a good idea of the spectral evolution. It is important to realize that only the nonoverlapping windows provide truly independent spectral information. But the overlapping ones permit us to check the continuous nature of

the spectral evolution, as well as providing better comparison with the visual information in the time series itself.

The results of ESA are visualized in Plate 1, with different colors for different levels of confidence. A few frequencies are fairly stable, i.e., they last for more than 30 kyr along the time axis in the figure, which means that they are stable for time intervals longer than 70 kyr in the signal, i.e., for nearly half the length of the record or more. The stable periods are 19.6, 11.4, 5.8, 4.4, 3.5, 2.7, and 2.4 kyr. These periods were calculated by a least squares fit of the frequency values on the ESA diagram, weighted by the confidence value derived from the F test. All these cycles are combination tones of f_1, f_2 and f_3 with positive coefficients and orders not exceeding 8 (see Table 3). The period of 36.5 kyr cannot be trusted, since it is almost equal to the length of the window, while periods of 2 kyr and shorter are too close to the noise level of the spectrum for a reliable evaluation of their stability.

It is clear from Plate 1 that the stability in frequency of the peaks associated with combination tones is quite comparable to that of the orbital peaks. We tested this further by using different types of prewhitening, e.g., centered differences
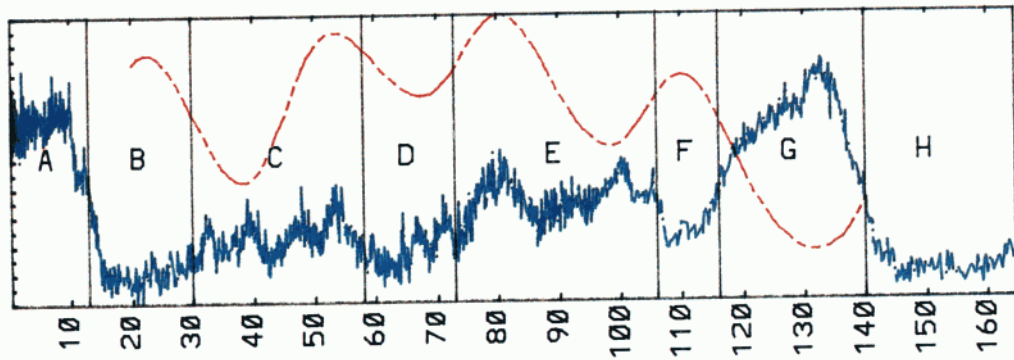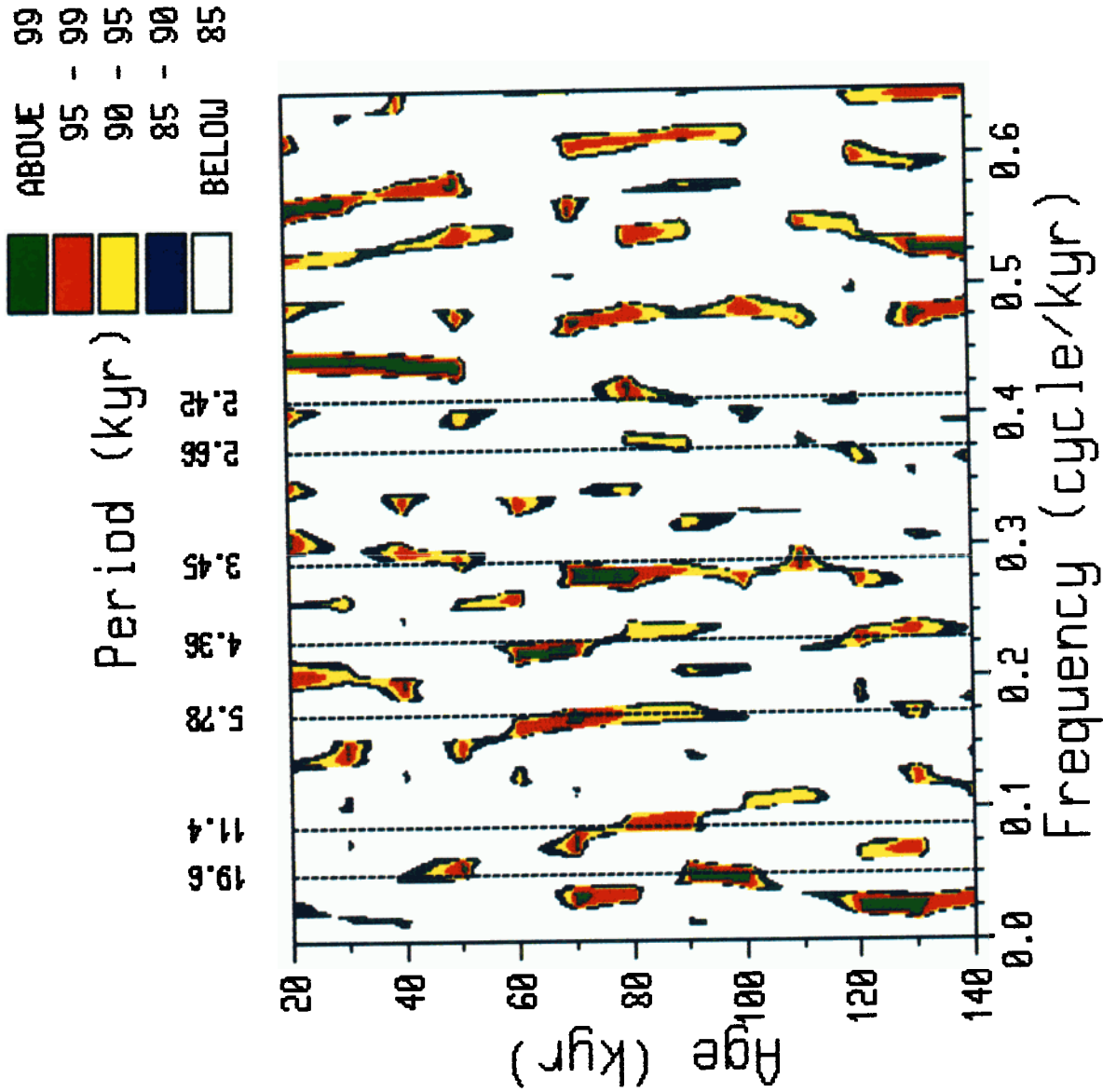
Plate 1. ESA analysis of the temperature time series at Vostok. The left axis represents the middle of the moving windows and the colors give the degree of confidence. The corresponding temperature time series is plotted on the left, in blue. The global high-frequency variability of the time series is plotted on the same scale, for comparison purposes, in red.

TABLE 3. Dynamically Stable Frequencies in the Vostok
Temperature Record

Period, kyr	Frequency, cycles/kyr	Combination Tone	Relative Error	Order of Combination
19.6	0.051	f_1	3×10^{-2}	1
11.4	0.088	$2f_2$	7×10^{-3}	2
5.78	0.173	$2f_1 + f_2 + f_3$	6×10^{-5}	4
4.36	0.229	$3f_1 + 3f_3$	8×10^{-3}	6
3.45	0.289	$3f_1 + 3f_2$	4×10^{-3}	6
2.66	0.376	$3f_1 + 5f_2$	2×10^{-3}	8
2.42	0.413	$7f_1 + f_2$	2×10^{-3}	8

The frequencies listed here were obtained by a least squares fit of
the frequencies found to be stable by ESA (see text for details).

instead of forward differences. The results (not shown) are
practically indistinguishable from those in Plate 1.

Some of the frequencies which appear to be stable, by
their duration, seem to exhibit a drift in frequency. We
attribute this phenomenon to local inaccuracies in the chro-
nology due to imperfections in the dating process. Hence
ESA based on MTM provides a tool for chronology testing
[*Benoist*, 1986] in that a "good" chronology should only
produce straight ridges, parallel to the time axis, in a
time-frequency diagram like Plate 1.

To test the stability of our results to changes in the *Lorius
et al.* [1985] chronology, we introduce a random perturbation
into it by adding pseudo-Gaussian noise to the date of every
ice sample in the core. The standard deviation of this noise
is taken equal to 10% of the estimated length of the time
interval between that sample and the one above it, in
accordance with the original error estimate of 5–10% of
Lorius et al. [1985], now confirmed by ^{10}Be data from
Vostok and two other Antarctic cores [*Jouzel et al.*, 1989].
The shape of the correspondingly modified evolutive spec-
trum (not shown) is hardly altered from Plate 1, which
proves the robustness of our results. On the other hand, a
perturbation with 20% standard deviation (not shown) does
produce substantial distortions of the time frequency dia-
gram.

It is beyond the purpose of the present paper to settle the
apparent discrepancies between the SPECMAP date of 128
ka ± 3 kyr for termination II [*Imbrie et al.*, 1991] and the
Jouzel et al. [1989] date of 138 ka ± 3 kyr for the G/H
boundary in the Vostok records. We merely note here the
following: the two chronologies agree quite well down to 110
ka [*Jouzel et al.*, 1989; *Imbrie et al.*, 1989]. Let us suppose
that the *Lorius et al.* [1985] chronology would erroneously
be "stretched" by 10 kyr between 110 and 140 ka, i.e., that
the true time interval covered roughly by interglacial G in the
Vostok records is 20 kyr rather than 30 kyr, as assumed
here. Then ESA would have to exhibit a shift of all signifi-
cant frequencies (shown in color) between the window
centered at 110 ka in Plate 1 and that at 140 ka (the last), by
a factor of 20 kyr/30 kyr = 2/3 to the left. No such systematic
shift is apparent in the figure. We can conclude only that
ESA results presented here buttress the Vostok chronology
[*Lorius et al.*, 1985; *Jouzel et al.*, 1989].

In order to get a better estimate of the effect of finite
sample length on the location of the peaks for the global
spectra, a GLT model simulation is also subjected to ESA.
The simulation is of 11 × 164 kyr = 1804 kyr, approximately
the total length of the Quaternary, and the window length of

164 kyr. The frequency band chosen this time lies between 0
and 0.1 cycles/kyr so as to include only orbital peaks and the
low-order combination tones ($N_i \leq 2$). The fluctuations in
period are between 95.2 and 111.1 kyr, for the $f_1 - f_2$ tone
centered at 105.3 kyr, and 10.3–10.6 kyr for $f_1 + f_2$, with
mean 10.4 kyr. The corresponding relative errors between
the mean from 11 realizations and the exact combination
tone are as large as 0.02. The fluctuations in the model
simulations are therefore quite comparable to the differences
in location of peaks between Figures 2a, 2b, and 2c, while
the relative errors are as large as those in Table 3.

For each time window, we also calculate the high-
frequency variability (HFV), i.e., the ratio of the power
spectrum in the frequency band between (1/15) cycles/kyr
and (1/2) cycles/kyr, with respect to the total power spec-
trum between 0 and 0.65 cycles/kyr. These values are
smoothed with a cubic spline and plotted along with the
temperature time series itself against the ESA diagram (see
Plate 1). Keeping in mind that a single point on the HFV
curve represents an MTM analysis on 40 kyr, we find good
agreement with the visual inspection of the record: a long
interval of high variability in the stages C, D, and late E, and
an interval of lower variability in the early part of stage E, as
well as in stages F and G. The nature of the record and of
ESA does not permit extending the HFV curve into stage A,
to verify the visually large HFV there. The marked drop in
HFV toward the bottom of the core is due, at least in part, to
an undersampling of the core in those stages.

5. DISCUSSION AND CONCLUSIONS

The pioneering paper of *Hays et al.* [1976] opened new
horizons in paleoclimatology by emphasizing the role of
spectral information, which is more robust and hence phys-
ically more significant than time domain information. In fact,
nonlinear dynamics suggests that most natural phenomena
are aperiodic, and hence the timing of individual events is
both unpredictable and physically irrelevant [*Lorenz*, 1963;
Guckenheimer and Holmes, 1983]. The consequences of this
fact for the theory of Quaternary glaciations have been
explored in some detail by *Le Treut and Ghil* [1983], *Ghil
and Childress* [1987], *Le Treut et al.* [1988] and *Ghil* [1985,
1989].

In the present paper we have taken the spectral point of
view one step further, by investigating frequencies higher
than the orbital ones; such high frequencies characterize
climatic variability during the Holocene and the late Pleis-
tocene. This investigation was facilitated by the fortunate
coming together of better data and better spectral methods.
The data are provided by a continuous time series from the
Vostok ice core [*Lorius et al.*, 1985; *Jouzel et al.*, 1987],
covering the last 164 kyr with an average resolution of 100
years (Figure 1). The method is the multitaper method
(MTM) of *Thomson* [1982], which achieves high spectral
resolution for short time series, as well as estimating the
statistical significance of the detected peaks, independently
of their amplitude. *Hays et al.* [1976] were able to detect by
the Blackman-Tukey method peaks near 40 and 20 kyr in a
marine record which only displayed a near periodicity of 100
kyr in the time domain. Likewise, by using MTM, we were
able to detect a number of peaks between 2 and 15 kyr in an
ice core record which only displays near periodicities of 40
and 20 kyr in the time domain.

Applying MTM to the entire record, we confirmed first the presence of the orbital peaks near $f_1 = 1/19$, $f_2 = 1/23$ and $f_3 = 1/41$ cycles/kyr, two of which had been obtained already by *Jouzel et al.* [1987] using a maximum entropy method (MEM). Next, we detected a dozen statistically significant combination tones

$$f_i^{(d)} = \sum_{j=1}^{3} n_j^{(i)} f_j$$

of these frequencies between 2 kyr and 15 kyr, with an accuracy comparable to that of the orbital peaks themselves (Figures 2a and 3a and Table 1). Such combination tones had been predicted by the nonlinear climate model of *Ghil and Le Treut* [1981], GLT in the text. The high-frequency peaks in the Vostok record match those in the GLT model [*Ghil*, 1985; *Ghil and Childress*, 1987; *Le Treut et al.*, 1988; *Ghil*, 1989] (Figures 2b and 3b).

The GLT model is based on three equations for the global climate system, incorporating radiation balance, ice mass balance, and mechanical equilibrium of ice sheets and bedrock. Quantitative evaluation of the number of statistically significant degrees of freedom in paleoclimatic records of comparable length yields an estimate between 5 and 10 [*Vautard and Ghil*, 1989; *Ghil*, 1989]. In addition to the three climatic mechanisms incorporated in the GLT model, other mechanisms have been proposed and are, no doubt, important in explaining additional features of the record.

These important mechanisms include changes in the biogeochemical carbon cycle [*Broecker et al.*, 1985; *Barnola et al.*, 1987; *Saltzman*, 1987], detailed, active ice sheet and bedrock dynamics [*Birchfield and Grumbine*, 1985], ice sheet thermodynamics [*Oerlemans*, 1982], and changes in the thermohaline ocean circulation [*Stigebrandt*, 1985; *Ghil et al.*, 1987]. Together with the three mechanisms of GLT, the mechanisms above can make up the requisite number of 5–10 [*Ghil*, 1989]. While it is not claimed that the GLT model provides anything like a full explanation of late Quaternary glaciations, the verification of its combination-tone prediction does illustrate the power of nonlinear dynamics, in general, and of simple nonlinear climate models, in particular. This prediction is verified here with a very high degree of certainty (Table 2).

Evolutive spectral analysis (ESA) with the MTM method permits the study of the dynamic stability, in time, of peaks detected by analyzing the entire record. Of the dozen high frequencies detected by global MTM (Table 1), ESA confirms the dynamic stability of about half that number (Table 3). Global analysis detected two peaks which did not appear to be low-order combination tones of the orbital frequencies, and three combination tones whose order

$$N_i = \sum_{j=1}^{3} |n_j^{(i)}|$$

did not increase monotonically with frequency. ESA retains only combination tones, and their order does increase monotonically with frequency.

Of these tones we note the second harmonic of an orbital peak, $2f_2$, and the third harmonic, at 3.5 kyr, of 10.4 kyr = $1/(f_1 + f_2)$, particularly prominent in the GLT results [*Le*

Treut and Ghil, 1983; *Ghil*, 1985; *Le Treut et al.*, 1988]. The well-known ice core peak near 2.5 kyr [*Dansgaard et al.*, 1971; *Benoist et al.*, 1982] appears to split into two sharp peaks, near 2.7 and 2.4 kyr. *Pestiaux et al.* [1988] had also detected two combination tones near 2.5 kyr in their marine cores, but their respective orders were both 9, rather than 8, confirming the better resolution of the Vostok record and the sharper discrimination of our spectral methods.

The total high-frequency variability (HFV) of the Vostok temperature in 40 kyr windows (Plate 1) exhibits a systematic change in time over the record. The intervals of high and low HFV also support the role of internal climatic mechanisms over the last full glacial cycle, since no HFV nor changes in it are present over this time interval in the orbital parameters. The frequencies of the superorbital peaks, like the orbital ones, are reasonably stable, while the relative importance of the distinct peaks, in terms of amplitude (not shown) and statistical significance (Plate 1) changes. This behavior strongly suggests that the underlying climatic system does undergo self-induced transitions between different types of behavior [*Lorenz*, 1968; *Ghil*, 1984; *Saltzman and Sutera*, 1987], while the external forcing is essentially the same.

We conclude that a small number of nonlinear feedback mechanisms play a crucial role in paleoclimatic variability. These nonlinearities may extend the range of orbital influences to periodicities as short as 2 kyr.

Better discrimination between the climatic mechanisms most responsible for this nonlinear variability requires careful intercomparisons between marine and ice core records [*Le Treut et al.*, 1988]. These comparisons, in turn, require considerable attention to chronology problems which evolutive spectral analysis can help to solve.

APPENDIX A: MULTITAPER SPECTRAL METHOD

The purpose of this nonparametric spectral method [*Thomson*, 1982] is to model a time series $\{x(i): i = 0, \cdots, N - 1\}$ by a finite sum of sinusoids of angular frequencies $\{\omega(j): j = 0, \cdots, P - 1\}$ and to calculate the corresponding amplitudes by a least squares procedure. A statistical test for the significance of the model is also provided.

Boldface letters will refer to vectors containing the signal or the tapers or to matrices. So $\mathbf{x} \cdot \mathbf{w}$ means the scalar product of the vectors $\mathbf{x} = (x(0), \cdots, x(N - 1))$ and $\mathbf{w} = (w(0), \cdots, w(N - 1))$. Roman letters refer to real or complex scalars.

Optimal Choice of Tapers

Assume that $\mathbf{x}$ is a sinusoidal signal of angular frequency $\hat{\omega}$, i.e., $x(t) = \mu e^{i\hat{\omega}t}$ for $t = 0, \cdots, N - 1$. Then let $\{w(t)\}_{t=0\cdots N-1}$ be a taper of length N and $\mathbf{y}$ the discrete Fourier transform (DFT) of the tapered signal $\mathbf{x} \cdot \mathbf{w}$:

$$y(\omega) = \sum_{t=0}^{N-1} x(t)w(t)e^{-i\omega t}; \qquad (A1)$$

here, $\omega = k/N$ with $k = 0, \cdots, P - 1$.

The primary purpose of the taper is to minimize spectral leakage, i.e., to minimize the energy contribution outside a given bandwidth ($\hat{\omega} - \Omega$, $\hat{\omega} + \Omega$) from the tapered signal with angular frequency $\hat{\omega}$, where $|y(\omega)|^2$ is an estimate of the

power of the signal. Thus the tapered signal $x \cdot w$ should have as much of its energy as possible in $(\hat{\omega} - \Omega, \hat{\omega} + \Omega)$, relative to its total power which covers the entire band $(-\pi, \pi)$. Hence we choose a taper w so as to maximize the function

$$F(\mathbf{w}) = \frac{\displaystyle\int_{\hat{\omega} - \Omega}^{\hat{\omega} + \Omega} |y(\omega)|^2 \, d\omega}{\displaystyle\int_{-\pi}^{\pi} |y(\omega)|^2 \, d\omega}. \qquad (A2)$$

Substituting (A1) into (A2), one obtains

$$F(\mathbf{w}) = \frac{\mathbf{w} \cdot \mathbf{A} \cdot \mathbf{w}}{\mathbf{w} \cdot \mathbf{w}}, \qquad (A3)$$

where $\mathbf{A}$ is an $N \times N$ symmetric positive definite matrix, and

$$\mathbf{A}_{ij} = \frac{\sin \Omega(i - j)}{\pi(i - j)}, \qquad i \neq j,$$

$$\mathbf{A}_{ij} = \frac{\Omega}{\pi}, \qquad i = j. \qquad (A4)$$

Maximizing F with respect to $\mathbf{w}$ is thus a Rayleigh-Ritz problem. It is equivalent to the eigenvalue problem

$$\mathbf{A} \cdot \mathbf{w} = \lambda \mathbf{w}. \qquad (A5)$$

The eigenvectors $\mathbf{w}_k$ of this problem were called discrete prolate spheroidal sequences (DPSS) by *Slepian* [1978]. Order the tapers $\mathbf{w}_k$ by their associated eigenvalues λ_k,

$$1 > \lambda_0 \cdots \lambda_{N-1} > 0.$$

The expression $1 - \lambda_k$ gives the fraction of the total energy of the kth window outside the interval $(\hat{\omega} - \Omega, \hat{\omega} + \Omega)$. The first $2N\Omega$ tapers are known to have the best spectral properties, as they are very close to 1. Hence we use the first $K = \lfloor 2N\Omega \rfloor$ DPSS for our multitaper harmonic analysis where $[Z]$ stands for the integer part of Z.

Harmonic Analysis

Assume now that the signal x is the sum of a sinusoid of angular frequency $\hat{\omega}$ and amplitude μ, and a noise e which is the sum of other sinusoids and white noise. One can write

$$x(t) = \mu e^{i\hat{\omega}t} + e(t). \qquad (A6)$$

Let $\{w_k\}_{k=0 \cdots K-1}$ be the K first DPSS, $y_k(\omega)$ the DFT of $x \cdot w_k$, $U_k(\omega)$ the DFT of w_k and $e_k(\omega)$ the DFT of $e \cdot w_k$. Then we have

$$y_k(\omega) = \sum_{t=0}^{N-1} x(t) w_k(t) e^{-i\omega t}, \qquad (A7a)$$

$$U_k(\omega) = \sum_{t=0}^{N-1} w_k(t) e^{-i\omega t}, \qquad (A7b)$$

$$e_k(\omega) = y_k(\omega) - \mu \sum_{t=0}^{N-1} w_k(t) e^{i(\hat{\omega} - \omega)t}. \qquad (A7c)$$

Choosing $\omega = \hat{\omega}$ in (A7c) one has

$$e_k(\hat{\omega}) = y_k(\hat{\omega}) - \mu U_k(0). \qquad (A8)$$

We want to minimize the noise contribution in the model (A6), i.e., to minimize the quantity

$$\sum_{k=0}^{K-1} |e_k(\hat{\omega})|^2 \qquad (A9)$$

as a function of μ.

By equating the derivative of (A9) with respect to μ at $\omega = \hat{\omega}$ to zero, we obtain an estimate $\hat{\mu}$ of μ:

$$\hat{\mu}(\hat{\omega}) = \frac{\displaystyle\sum_{k=0}^{K-1} U_k^*(0) y_k(\hat{\omega})}{\displaystyle\sum_{k=0}^{K-1} |U_k(0)|^2}, \qquad (10)$$

where the asterisk denotes complex conjugation. Equation (A10) yields a least squares fit, and hence the statistical confidence can be measured by a Fisher test. This test is based roughly on the ratio of the variance explained by the model (A6) to the unexplained variance. By expanding the variance of the model, one finds that it is the sum of two terms:

$$\theta = |\hat{\mu}(\hat{\omega})|^2 \sum_{k=0}^{K-1} |U_k(0)|^2, \qquad (A11a)$$

$$\psi = \sum_{k=0}^{K-1} |y_k(\hat{\omega}) - \hat{\mu}(\hat{\omega}) U_k(0)|^2, \qquad (A11b)$$

which are the explained and unexplained contributions to the variance, respectively.

The random variable

$$F(\hat{\omega}) = (K - 1) \frac{\theta}{\psi} \qquad (A12)$$

follows a Fisher-Snedecor law with 2 and $2K - 2$ degrees of freedom. One can interpret its value by assuming that $\mu = 0$ and trying to reject this hypothesis with the lowest probability of failure. For instance, if $F > 3.11$, one can reject the hypothesis $\mu = 0$ with less than 10% chance to make a mistake. This method is able to detect low-amplitude oscillations with a high degree of statistical significance or to reject a large amplitude if it failed the F test.

REFERENCES

Anderson, R. Y., A long geoclimatic record from the Permian, *J. Geophys. Res.*, *87*, 7285–7294, 1982.

Bard, E., M. Arnold, J. Duprat, J. Moyes, and J.-C. Duplessy, Reconstruction of the last deglaciation: Deconvolved records of $\delta^{18}O$ profiles, micropaleontological variations and accelerator mass spectrometric ^{14}C dating, *Clim. Dyn.*, *1*, 101–112, 1987.

Barnola, J. M., D. Raynaud, Y. N. Korotkevitch, and C. Lorius, Vostok ice core provides 160,000-year record of atmospheric CO_2, *Nature*, *329*, 408–414, 1987.

Benoist, J. P., Analyse spectrale de signaux glaciologiques: Etude des glaces sédimentaires deposées à Dome C: Morphologie du lit d'un glacier, Ph.D. thesis, Univ. Sci., Med. of Tech., Grenoble, France, 1986.

Benoist, J. P., F. Glangeaud, N. Martin, J. L. Lacoume, C. Lorius, and A. Ait Oulahman, Study of climatic time series by time-frequency analysis, in *Proceedings of the ICASSP82*, vol. 3, pp. 1902–1905, Institute of Electrical and Electronics Engineers, New York, 1982.

Berger, A. L., Long-term variations of daily insolation and Quaternary climatic changes, *J. Atmos. Sci.*, *35*, 2362–2367, 1978.

Birchfield, G. E., and R. W. Grumbine, "Slow" physics of large continental ice sheets and underlying bedrock, and its relation to the Pleistocene ice ages, *J. Geophys. Res.*, *90*, 11,294–11,302, 1985.

Broecker, W. S., Terminations, in *Milankovitch and Climate: Understanding the Response to Astronomical Forcing*, edited by A. Berger, et al., pp. 687–698, D. Reidel, Hingham, Mass., 1984.

Broecker, W. S., D. M. Peteet, and D. Rind, Does the ocean-atmosphere system have more than one stable mode of operation?, *Nature*, *315*, 21–25, 1985.

Dansgaard, W., S. J. Johnsen, H. B. Clausen, D. Dahl-Jensen, and C. J. Langway, Climate records revealed by the Camp Century ice cores, in *The Late Cenozoic Glacial Ages*, edited by K. K. Turekian, pp. 37–56, Yale University Press, New Haven, Conn., 1971.

Duplessy, J.-C., G. Delibrias, J. L. Turon, C. Pujol, and J. Duprat, Deglacial warming of the northeastern Atlantic Ocean— Correlation with the paleoclimatic evolution of the European continent, *Palaeogeogr. Palaeoclimatol. Palaeoecol.*, *35*, 121–144, 1981.

Ghil, M., Climate sensitivity, energy balance models, and oscillatory climate models, *J. Geophys. Res.*, *89*, 1280–1284, 1984.

Ghil, M., Theoretical climate dynamics: An introduction, in *Turbulence and Predictability in Geophysical Fluid Dynamics and Climate Dynamics*, edited by M. Ghil, R. Benzi, and G. Parisi, pp. 347–402, North-Holland, Amsterdam, 1985.

Ghil, M., Deceptively-simple models of climatic change, in *Climate and Geosciences*, edited by A. Berger et al., pp. 211–240, D. Reidel, Hingham, Mass., 1989.

Ghil, M., and S. Childress, *Topics in Geophysical Fluid Dynamics: Atmosphere Dynamics, Dynamo Theory and Climate Dynamics*, Springer-Verlag, New York, 1987.

Ghil, M., and H. Le Treut, A climate model with cryodynamics and geodynamics, *J. Geophys. Res.*, *86*, 5262–5270, 1981.

Ghil, M., A. Mullhaupt, and P. Pestiaux, Deep water formation and Quaternary glaciacions, *Clim. Dyn.*, *2*, 1–10, 1987.

Guckenheimer, J., and P. Holmes, *Nonlinear Oscillations, Dynamical Systems and Bifurcations of Vector Fluids*, Springer-Verlag, New York, 1983.

Hays, J. D., J. Imbrie, and N. J. Shackleton, Variations in the Earth's orbit: Pacemaker of the ice ages, *Science*, *194*, 1121–1132, 1976.

Held, I. M., Climate models and the astronomical theory of the ice ages, *Icarus*, *50*, 449–461, 1982.

Imbrie, J., and K. P. Imbrie, *Ice Ages: Solving the Mystery*, 2nd ed., Harvard University Press, Cambridge, Mass., 1986.

Imbrie, J., J. D. Hays, D. J. Martinson, A. McIntyre, A. C. Mix, J. J. Morley, N. G. Pisias, W. L. Prell, and N. J. Shackleton, The orbital theory of Pleistocene climate: Support from a revised chronology of the marine $\delta^{18}O$ record, in *Milankovitch and Climate: Understanding the Response to Astronomical Forcing*, edited by A. Berger, et al., pp. 269–305, D. Reidel, Hingham, Mass., 1984.

Imbrie, J., A. McIntyre, and A. Mix, Oceanic response to orbital forcing in the late Quaternary, observational and experimental

strategies, in *Climate and Geosciences*, edited by A. Berger et al., pp. 121–164, D. Reidel, Hingham, Mass., 1989.

Jenkins, G. M., and D. G. Watts, *Spectral Analysis and Its Applications*, Holden Day, Oakland, Calif., 1968.

Jouzel, J., and L. Merlivat, Deuterium and oxygen 18 in precipitation: Modeling of the isotopic effects during snow formation, *J. Geophys. Res.*, *89*, 11,749–11,757, 1984.

Jouzel, J., C. Lorius, J. R. Petit, C. Genthon, N. I. Barkov, V. M. Kotlyakov, and V. M. Petrov, Vostok ice core: A continuous temperature record over the last climatic cycle (160,000 years), *Nature*, *329*, 403–408, 1987.

Jouzel, J., G. Raisbeck, J.-P. Benoist, F. Yiou, C. Lorius, D. Raynaud, J.-R. Petit, N. I. Barkov, Y. S. Korotkevitch, and V. M. Kotlyakov, A comparison of deep Antarctic ice cores and their implications for climate between 65,000 and 15,000 years ago, *Quat. Res.*, *31*, 135–150, 1989.

Kallel, N., L. D. Labeyrie, M. Arnold, H. Okada, W. C. Dudley, and J.-C. Duplessy, Evidence of cooling during the Younger Dryas in the western North Pacific, *Oceanol. Acta*, *11*, 369–375, 1988.

Kay, S. M., and S. L. Marple, Spectrum analysis—A modern perspective, *Proc. IEEE*, *69*, 1380–1419, 1981.

Le Treut, H., and M. Ghil, Orbital forcing, climatic interactions, and glaciation cycles, *J. Geophys. Res.*, *88*, 5167–5190, 1983.

Le Treut, H., J. Portes, J. Jouzel, and M. Ghil, Isotopic modeling of climatic oscillations: Implications for a comparative study of marine and ice core records, *J. Geophys. Res.*, *93*, 9365–9383, 1988.

Lorenz, E. N., Deterministic nonperiodic flow, *J. Atmos. Sci.*, *20*, 130–141, 1963.

Lorenz, E. N., Climatic determinism, *Meteorol. Monogr.*, *8*(30), 1–3, 1968.

Lorius, C., and L. Merlivat, Distribution of mean surface stable isotope values in East Antarctica; observed changes with depth in a coastal area, in Isotopes and Impurities in Snow and Ice, Proceedings Grenoble Symposium, *IAHS Publ.*, *118*, 127–137, 1977.

Lorius, C., J. Jouzel, C. Ritz, L. Merlivat, N. I. Barkov, M. Kotlyakov, and V. M. Petrov, A 150,000 year climatic record from Antarctic ice, *Nature*, *316*, 591–596, 1985.

Milankovitch, M., Kanon der Erdbestrahlung und seine Anwendung auf das Eiszeitenproblem, *R. Serb. Acad., Spec. Publ. 133*, pp. 1–633, Belgrade, 1941. (English translation, Israel Program for Scientific Translation, Jerusalem, 1969.)

Nelson, C. S., C. H. Hendy, G. R. Jarett, and A. M. Cuthberson, Near-synchroneity of New Zealand alpine glaciations and northern hemisphere continental glaciations during the past 750 kyr, *Nature*, *318*, 361–363, 1985.

Oerlemans, J., Glacial cycles and ice sheet modelling, *Clim. Change*, *4*, 353–374, 1982.

Olsen, P. E., A 40-million-year lake record of early Mesozoic orbital climatic forcing, *Science*, *234*, 842–848, 1986.

Park, J., C. R. Lindberg, and F. L. Vernon III, Multitaper spectral analysis of high-frequency seismograms, *J. Geophys. Res.*, *92*, 12,675–12,684, 1987.

Peltier, R., Dynamics of the ice age Earth, *Adv. Geophys.*, *24*, 1–146, 1982.

Pestiaux, P., Approche spectrale en modélisation paléoclimatique, Ph.D. thesis, Univ. Cath. de Louvain, Louvain, Belgium, 1984.

Pestiaux, P., I. Van Der Mersch, A. Berger, and J. C. Duplessy, Paleoclimatic variability at frequencies ranging from 1 cycle per 10,000 years to 1 cycle per 1000 years: Evidence for nonlinear behaviour of the climate system, *Clim. Change*, *12*, 9–37, 1988.

Petit, J.-R., L. Mounier, J. Jouzel, Y. S. Korotkevitch, V. I. Kotlyakov, and C. Lorius, Palaeoclimatological and chronological implications of the Vostok core dust record, *Nature*, *343*, 56–58, 1990.

Pisias, N. G., and T. C. Moore, The evolution of the Pleistocene climate, *Earth Planet. Sci. Lett.*, *52*, 458–465, 1981.

Pisias, N. G., and D. K. Rea, Late Pleistocene paleoclimatology of the central equatorial Pacific: Sea surface response to the southeast trade winds, *Paleoceanography*, *3*, 21–37, 1988.

Saltzman, B., Paleoclimatic modeling, in *Paleoclimate Analysis and Modeling*, edited by A. D. Hecht, pp. 341–396, John Wiley, New York, 1985.

Saltzman, B., Carbon dioxide and the $\delta^{18}O$ record of late-

Quaternary climatic change: A global model, *Clim. Dyn.*, *1*, 77–85, 1987.

Saltzman, B., and A. Sutera, The mid-Quaternary climatic transition as the free response of a three-variable dynamical model, *J. Atmos. Sci.*, *44*, 236–241, 1987.

Shackleton, N. J., and N. D. Opdyke, Oxygen isotope and paleomagnetic stratigraphy of the equatorial Pacific core V28-239; Late Pliocene to latest Pleistocene, *Mem. Geol. Soc. Am.*, *145*, 449–463, 1976.

Slepian, S., Prolate spheroidal wave functions, Fourier analysis and uncertainty-V: The discrete case, *Bell. Syst. Tech. J.*, 1371–1430, 1978.

Stigebrandt, A., On the hydrographic and ice condions in the northern North Atlantic during different phases of a glaciation cycle, *Paleogeogr. Paleoclimatol. Paleoecol.*, *50*, 303–321, 1985.

Thomson, D. J., Spectrum estimation and harmonic analysis, *Proc. IEEE*, *70*, 1055–1096, 1982.

Vautard, R., and M. Ghil, Singular spectrum analysis in nonlinear dynamics, with applications to paleoclimatic time series, *Physica D Amsterdam*, *35*, 395–424, 1989.

Winograd, I. J., B. J. Szabo, T. B. Coplen, and A. C. Riggs, A 250,000-year climatic record from Great Basin Vein Calcite: Implications for Milankovitch theory, *Science*, *242*, 1275–1280, 1988.

J. M. Barnola and C. Lorius, Laboratoire de Glaciologie et de Géophysique de l'Environnement, F-38402 Saint Martin d'Hères Cedex, France.

C. Genthon, J. Jouzel, and P. Yiou, Laboratoire de Géochimie Isotopique/IRDI/DESICP, Commissariat à l'Énergie Atomique, F-91191 Gif-sur-Yvette Cedex, France.

M. Ghil, Climate Dynamics Center, Department of Atmospheric Sciences, and Institute of Geophysics and Planetary Physics, University of California, Los Angeles, CA 90024.

Y. N. Korotkevitch, Arctic and Antarctic Research Institute, Beringa Street 38, 199226, Leningrad, USSR.

H. Le Treut, Laboratoire de Météorologie Dynamique, École Normale Supérieure/CNRS, F-75005 Paris Cedex, France.